Supporting information

Decoupling of Mechanical Strength and Ionic Conductivity in Zwitterionic Elastomer Gel Electrolyte towards Safe Batteries

Yan Liu, Lei Hou,* Yucong Jiao,* and Peiyi Wu*

State Key Laboratory for Modification of Chemical Fibers and Polymer Materials, College of Chemistry Chemical Engineering and Biotechnology, Donghua University, Shanghai 201620, China

E-mail: wupeiyi@dhu.edu.cn; yucong.jiao@dhu.edu.cn; houlei@dhu.edu.cn;

This material includes

Figure S10. Cycling stability of PMEA electrolyte for lithium symmetrical battery at current density of 1 mA cm^{-2}

Figure S11. SEM image of lithium anode of lithium symmetric battery with liquid electrolyte after cycling for 200 h at current density 1 mA cm^{-2}

Figure S12. SEM images of lithium anode of lithium symmetric cell with PMEA after cycling for 200 h at current density 1 mA cm^{-2}

Figure S13. (a) LSV curve of lithium symmetric cell with liquid electrolyte at a scan rate of 10 mV s^{-1}. (b) CV profiles of $LiFePO_4$/PV_1M_1GE/Li at a scan rate of 0.1 mV s^{-1} in a potential window from 2 to 4V. (c) rate performances of $LiFePO_4$/Li with liquid electrolyte at 0.5, 1, 2, 3, 5 C; (d) cycling performances of liquid electrolyte at 5 C

Figure S14. Cycle stability of $LiFePO_4$/Li cell with PMEA at 5 C

Table S1. Comparison of electrochemical performance for PV_1M_1GE with other electrolytes

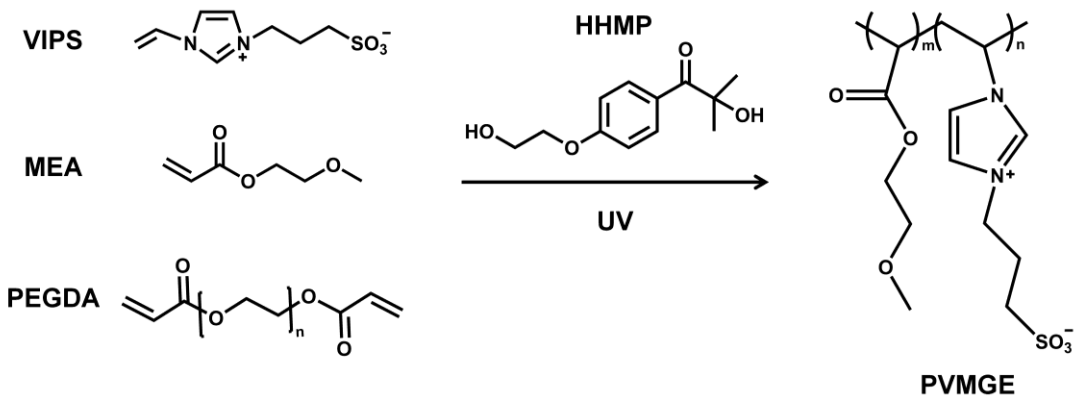

Figure S1. Molecular structures of PVMGE, VIPS, MEA, PEGDA and HHMP.

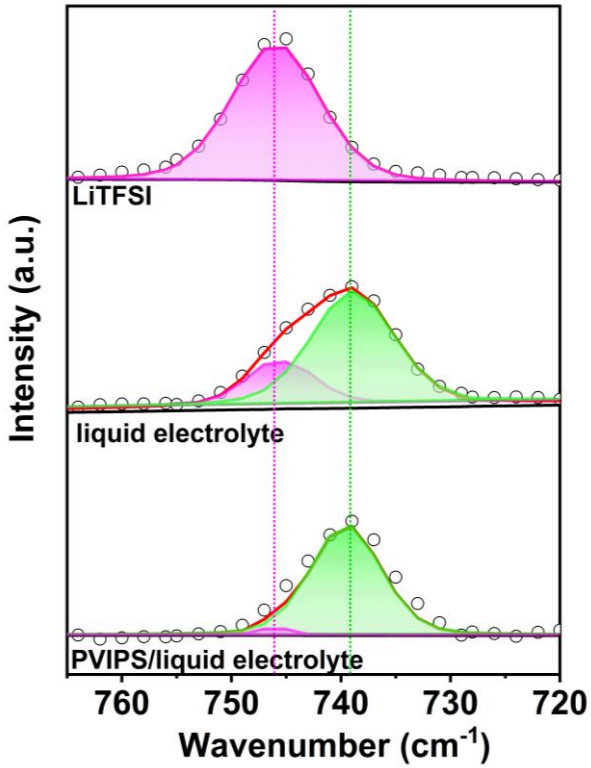

Figure S2. Raman spectra characterizing the dissociation effect of PVIPS on LiTFSI. The band at 739 cm^{-1} is related to uncoordinated $TFSI^-$ while the band at 746 cm^{-1} is related to bonded ion pairs. The ratio of uncoordinated $TFSI^-$ anions and bonded ion pairs is 0.76 in liquid electrolyte and 0.93 in PVIPS/liquid electrolyte, respectively.

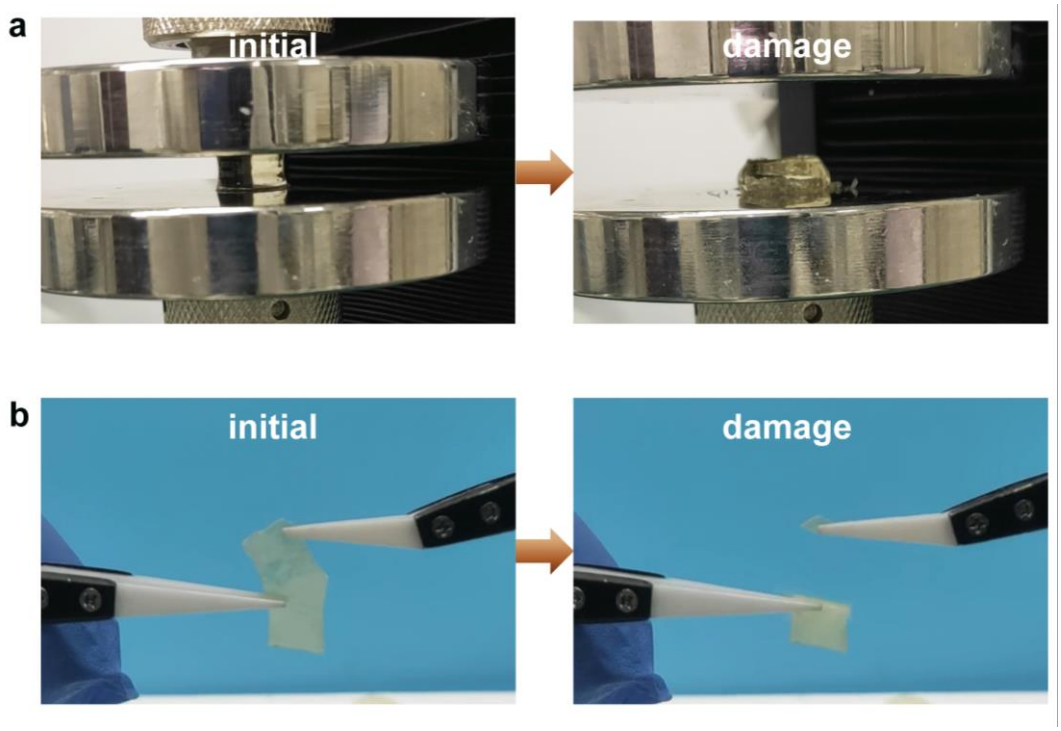

Figure S3. (a) Images of PV_4M_3GE before and after the compression; (b) exhibition of the brittleness of PVIPS gel electrolyte.

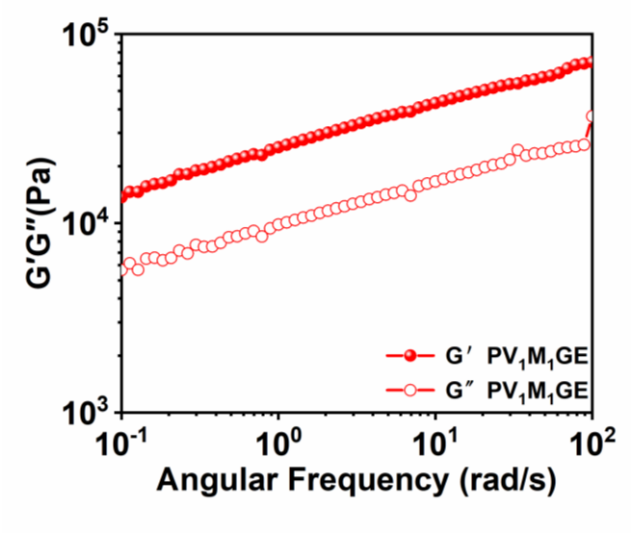

Figure S4. Frequency dependencies of the storage (G') and loss (G'') moduli of PV_1M_1GE.

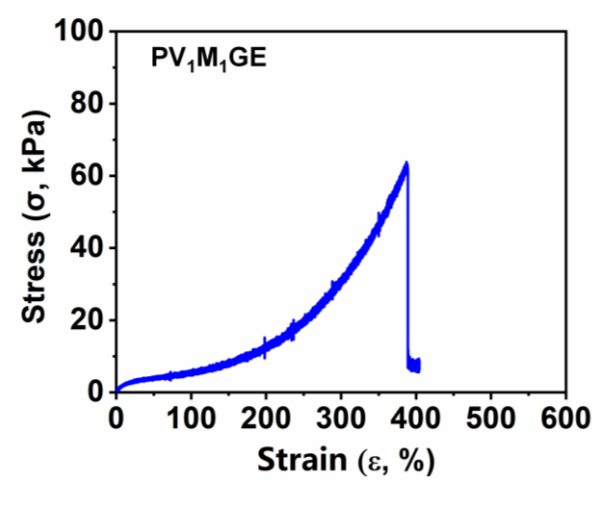

Figure S5. Tensile test of the PV_1M_1GE.

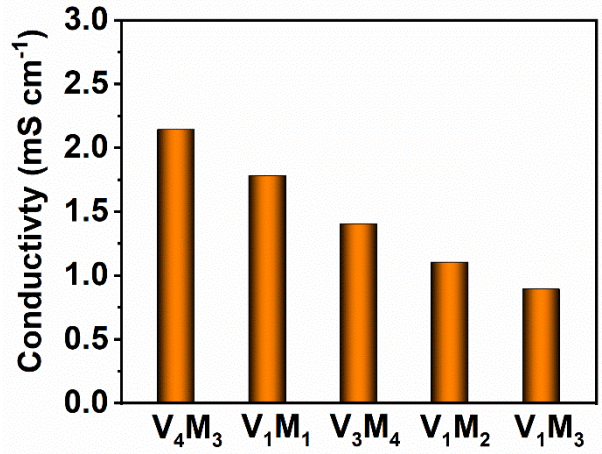

Figure S6. Ionic conductivity of the PVMGEs with different VIPS/MEA weight ratios.

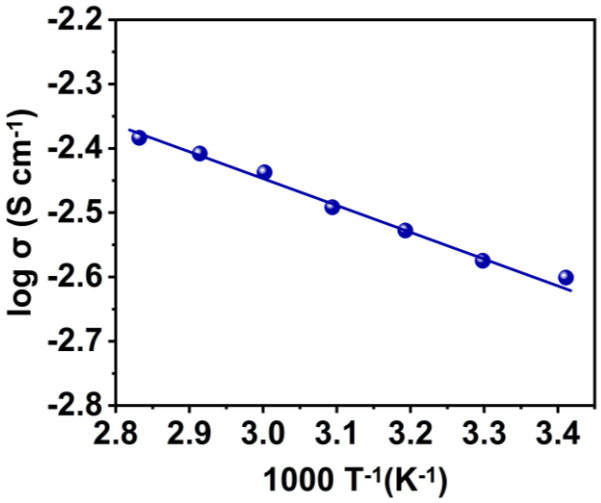

Figure S7. Temperature dependence of ionic conductivity of PV_1M_1GE.

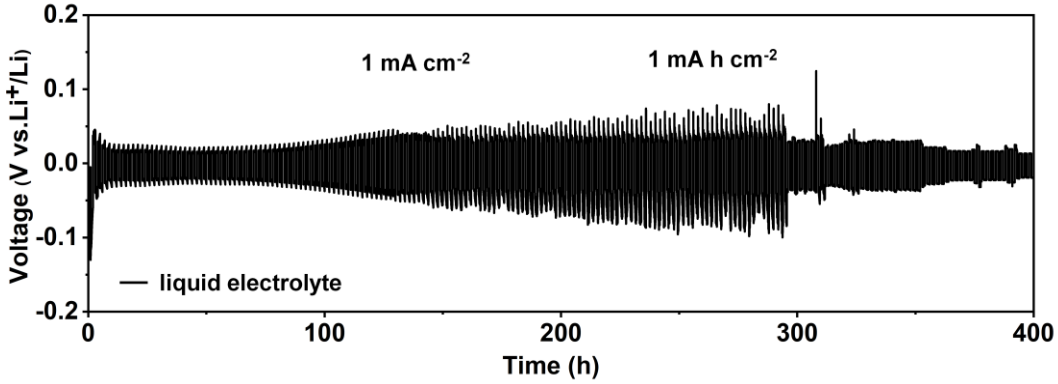

Figure S8. Li plating/stripping voltage profiles of lithium symmetric cells with liquid electrolyte at a current density of 1 mA cm^{-2}.

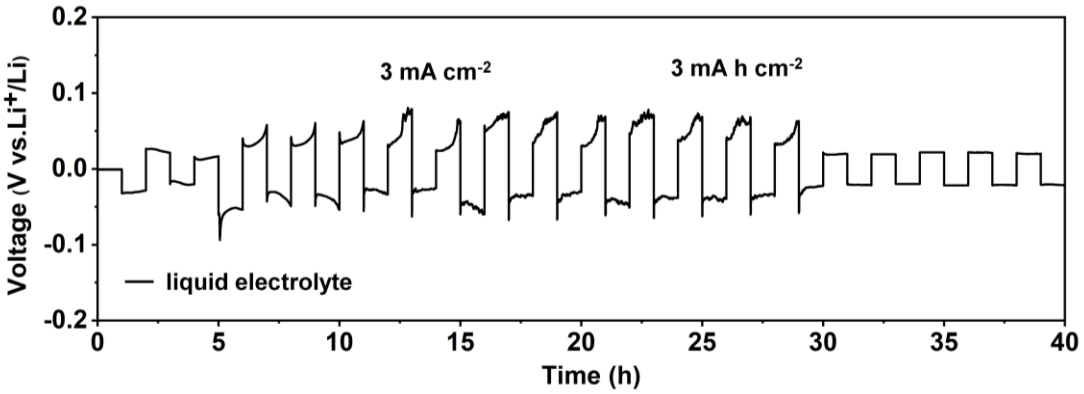

Figure S9. Cycling stability of lithium symmetric cell with liquid electrolyte at a current density of 3 mA cm^{-2}.

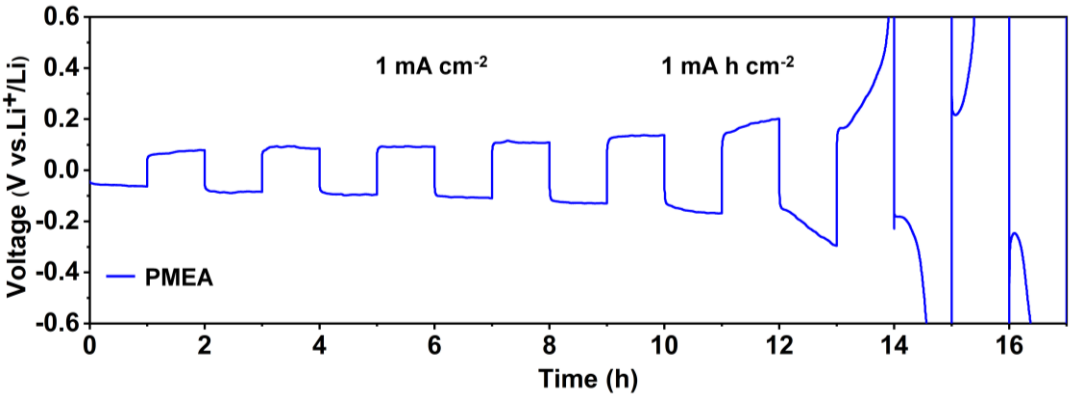

Figure S10. Cycling stability of PMEA electrolyte for lithium symmetrical battery at current density of 1 mA cm^{-2}.

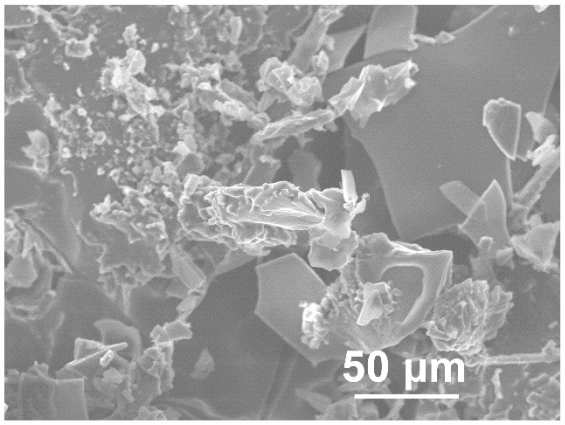

Figure S11. SEM image of lithium anode of lithium symmetric battery with liquid electrolyte after cycling for 200 h at current density 1 mA cm^{-2}.

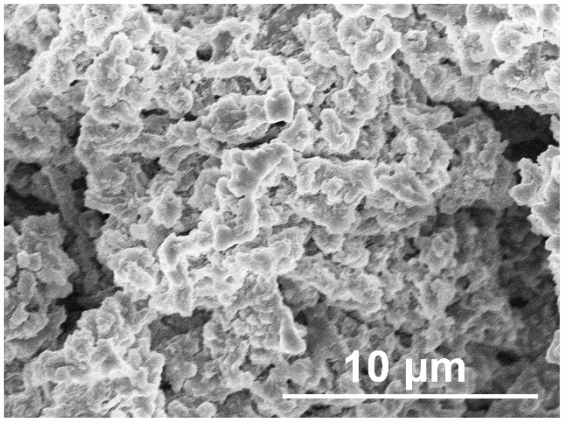

Figure S12. SEM images of lithium anode of Li/PMEA/Li cell after cycling for 200 h at current density 1 mA cm^{-2}.

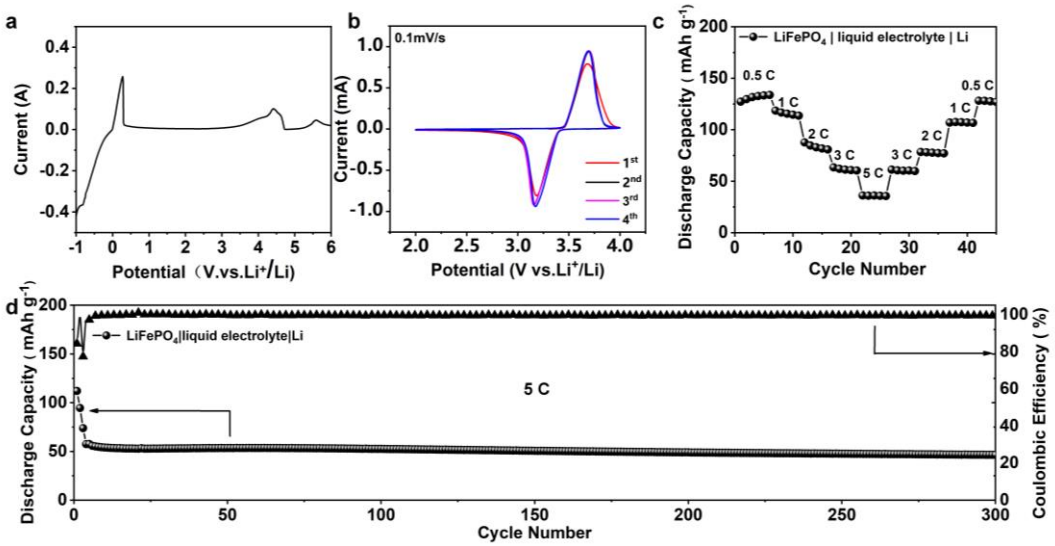

Figure S13. (a) LSV curve of lithium symmetric cell with liquid electrolyte at a scan rate of 10 mV s^{-1}. (b) CV profiles of $LiFePO_4/PV_1M_1GE/Li$ at a scan rate of 0.1 mV s^{-1} in a potential window from 2 to 4V. (c) rate performances of $LiFePO_4$/Li with liquid electrolyte at 0.5, 1, 2, 3, 5 C; (d) cycling performances of liquid electrolyte at 5 C.

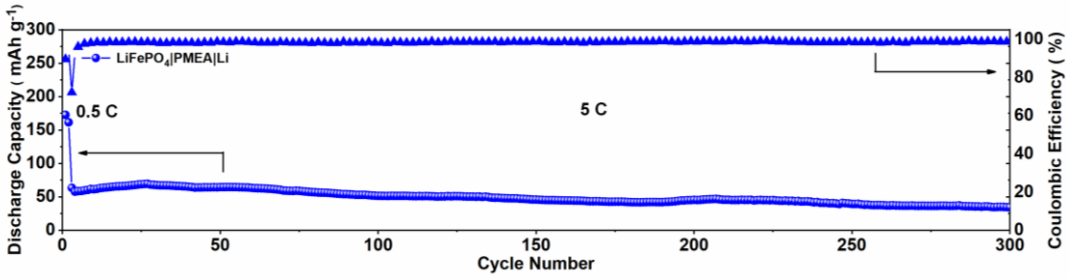

Figure S14. Cycling performance of $LiFePO_4$/Li cell with PMEA electrolyte at 5 C.

Table S1. Comparison of electrochemical performance for PV_1M_1GE with other electrolytes.

GPE	Li/Li		$LiFePO_4$/Li		Ref.
	Current density (mA cm^{-2})	Cycle Lifespans (h)	Current density (1 C=170 mA g^{-1})	Discharge capacity (mA h g^{-1})	
PV_1M_1GE	1	700	5 C	70	Our work
PVDF- HFP	1	250	2 C	57	1
SiO_2-GPE	1	400	0.1 C	125	2
glass fiber- poly (butyl acrylate)	0.5	~250	0.5 C	84	3
PAN-PEO	-	-	0.1 C	149	4
cellulose aerogel membranes	-	-	0.5 C	134	5
double polymer network-GPE	0.5	<400	0.5	124	6

References

(1) Li, L.; Wang, M.; Wang, J.; Ye, F.; Wang, S.; Xu, Y.; Liu, J.; Xu, G.; Zhang, Y.; Zhang, Y.; Yan, C.; Medhekar, N. V.; Liu, M.; Zhang, Y. Asymmetric Gel Polymer Electrolyte with High Lithium Ion Conductivity for Dendrite-Free Lithium Metal Batteries. *J. Mater. Chem. A* **2020,** *8*, 8033-8040.

(2) Yang, P.; Gao, X.; Tian, X.; Shu, C.; Yi, Y.; Liu, P.; Wang, T.; Qu, L.; Tian, B.; Li, M.; Tang, W.; Yang, B.; Goodenough, J. B. Upgrading Traditional Organic Electrolytes toward Future Lithium Metal Batteries: A Hierarchical Nano-SiO2-Supported Gel Polymer Electrolyte. *ACS Energy Lett.* **2020,** *5*,

1681-1688.

(3) Wu, S.; Zheng, H.; Tian, R.; Hei, Z.; Liu, H.; Duan, H. In-Situ Preparation of Gel Polymer Electrolyte with Glass Fiber Membrane for Lithium Batteries. *J. Power Sources* **2020,** *472*, 228627.

(4) Kuo, P. L.; Wu, C. A.; Lu, C. Y.; Tsao, C. H.; Hsu, C. H.; Hou, S. S. High Performance of Transferring Lithium Ion for Polyacrylonitrile-Interpenetrating Crosslinked Polyoxyethylene Network as Gel polymer Electrolyte. *ACS Appl. Mater. Interfaces* **2014,** *6*, 3156-3162.

(5) Wan, J.; Zhang, J.; Yu, J.; Zhang, J. Cellulose Aerogel Membranes with a Tunable Nanoporous Network as a Matrix of Gel Polymer Electrolytes for Safer Lithium-Ion Batteries. *ACS Appl. Mater. Interfaces* **2017,** *9*, 24591-24599.

(6) Zuo, T. T.; Shi, Y.; Wu, X. W.; Wang, P. F.; Wang, S. H.; Yin, Y. X.; Wang, W. P.; Ma, Q.; Zeng, X. X.; Ye, H.; Wen, R.; Guo, Y. G. Constructing a Stable Lithium Metal-Gel Electrolyte Interface for Quasi-Solid-State Lithium Batteries. *ACS Appl. Mater. Interfaces* **2018,** *10*, 30065-30070.